IEEE Access
Multidisciplinary | Rapid Review | Open Access Journal

Received 24 June 2022, accepted 6 July 2022, date of publication 7 July 2022, date of current version 18 July 2022.

Digital Object Identifier 10.1109/ACCESS.2022.3189573

Annular Ring Ultra Wideband Antenna Integrated With Metallic via Array for IoT Applications

INDERPREET KAUR[1], BANANI BASU[2], (Senior Member, IEEE), ANIL KUMAR SINGH[3], VINAY RISHIWAL[4], (Senior Member, IEEE), SUDEEP TANWAR[5], (Senior Member, IEEE), GULSHAN SHARMA[6], PITSHOU N. BOKORO[6], AND RAVI SHARMA[7]

[1]Department of Electronics and Communication, Mahatma Jyotiba Phule Rohilkhand University (MJPRU), Bareilly 243006, India
[2]Department of Electronics and Communication, National Institute of Technology Silchar (NIT Silchar), Silchar, Assam 788010, India
[3]Department of Electronics and Instrumentation, Mahatma Jyotiba Phule Rohilkhand University (MJPRU), Bareilly, Uttar Pradesh 243006, India
[4]Department of Computer Science and Information Technology, Mahatma Jyotiba Phule (MJP) Rohilkhand University, Bareilly 243006, India
[5]Department of Computer Science and Engineering, Institute of Technology, Nirma University, Ahmedabad, Gujarat 382481, India
[6]Department of Electrical Engineering Technology, University of Johannesburg, Johannesburg 2006, South Africa
[7]Centre for Inter-Disciplinary Research and Innovation, University of Petroleum and Energy Studies, Dehradun 248001, India

Corresponding authors: Inderpreet Kaur (inderpreet.mjpru@gmail.com) and Sudeep Tanwar (sudeep.tanwar@nirmauni.ac.in)

ABSTRACT An annular ring microstrip antenna (ARMSA) with metallic drilled holes and a defected ground structure is proposed for ultra-wideband applications. The annular ring microstrip patch antenna is excited by the microstrip line feed. The outer radius of the annular ring was optimized in this paper to choose the resonant frequency corresponding to the highest mode. The inner radius boosts the structure's gain. A defected conductive strip with an arc in the center increases bandwidth at the lower end, increases gain and suppresses Co and Cross-pole isolation. Incorporating a metallic via array excites and includes several closely spaced lower order modes, increasing the fractional bandwidth to 108%. The gain of the proposed configuration is 10dBi at the resonance frequency. It offers Front to back lobe ratio (FBR) of 34dB and 97% radiation efficiency. The performance of the fabricated prototype agrees well with the simulated one.

INDEX TERMS Annular ring microstrip antenna, front to back ratio, ultra wideband, defected ground structure.

I. INTRODUCTION

IoT continues its move into the mainstream, with billions of devices entering deployment. Organizations are moving from limited pilot projects to hyper-scale rollouts, depending on the business's digital future. Alongside connectivity and power, The antenna is how an IoT device receives and sends signals to the outside world and therefore is a fundamental element of an IoT device. Factors influencing the antenna selection for an IoT design are frequency band, size, range, precision, the region of deployment, etc. The IoT antenna operates in the unlicensed I.S.M. band (industrial, scientific, medical). With a specific application in mind like Wi-Fi or Bluetooth, wearable gaming devices, I.P. cameras, and so on are examples of consumer applications. In contrast, industrial applications such as smart cities, smart agriculture, and so on are examples of industrial applications. The antenna selected should be perfectly positioned in the product packaging. The antenna topology, which determines the antenna's bandwidth, radiation pattern, gain, and overall efficiency, is as important as the antenna size.

Motivation of UWB antenna design: Broadband antenna like Log periodic, Spiral antenna is dispersive. Pulse of small duration in nanoseconds, picoseconds can not pass through this type of antenna and have severe distortion. Very brief time-domain pulses are used in ultra-wideband radio technology. The signal's frequency domain is widened when these pulses are used. The signal having a bandwidth greater than 20% of its center frequency is referred to as a UWB signal. In 2002, the F.C.C. established a spectrum of operation for UWB. signals ranging from 3.1GHz to 10.6GHz. Because of its huge bandwidth, this technology has sparked interest in industry and research

The associate editor coordinating the review of this manuscript and approving it for publication was Sathish Kumar.

- The UWB system can offer better immunity to
- Low loss penetration UWB systems can penetrate obstacles and thus operate under both line-of-sight (L.O.S.) and non-line-of-sight (NLOS). [1]
- Due to an increase in the operating frequency, the UWB antenna is usually more compact than older narrow-band antennas.
- High precision ranging: Due to the nanosecond duration of typical UWB pulses, UWB systems have good time-domain resolution and can provide [2] centimeter accuracy for location and tracking applications.
- UWB systems can support more than 500 Mb/s data transmission rate within 10 m. [1]
- Also, they operate in an unlicensed spectrum which is less crowded than the licensed spectrum. [1]
- Coexistence: The unique character of low power spectral density allows the UWB system to coexist with other services such as cellular systems, wireless local area networks (WLAN), global positioning systems (G.P.S.), etc. [1]

Drawbacks of UWB: Perhaps the most limiting the factor is the power restriction that limits UWB operation to about 10m at around 100 Mbps. Other UWB systems with either short distance and higher bit rate or longer distance and lower bit rate are also possible. The current interest in UWB systems has been troublesome to generate and modulate these short pulses up until now. Recent advances in semiconductor process technology make it possible to integrate Ultra Wide Band (UWB) pulse generators in a cost-efficient manner and thus enable the widespread use of UWB systems. However, acquisition and synchronization of UWB systems are still an open issue, as tracking the very short pulses with sufficient precision is very difficult. It may be that the transmitter can be more accessible and use less power than narrowband transmitters. Still, the receiver must be able to demodulate the signal reasonably without using too much power and costing too much. This could prove to be a challenge, as the signal has a bandwidth of several GHz [1], [2].

Previously, the narrowband characteristic was a significant limitation, and it's a real challenge for researchers [3]. When it comes to antenna design, there are numerous issues that researchers must consider. In current scenarios, antennas are sophisticated in design. The size reduction of antennas is another essential and difficult topic for researchers in antenna design. The geometry of supporting devices through which antennas are supported can also alter the properties of these antennas. As a result, a high bandwidth antenna with the smallest size and a simple design is required. Lightweight, low profile, conformability to planar surfaces, and simple integration with planar circuits are advantages of the antenna. In [4], The authors have developed a structure for a tiny UWB monopole antenna for IoT applications. The important factor in obtaining a small size is carefully developing the architecture while retaining a satisfactory degree of electrical performance. The final design has a footprint of 175 mm^2 and dimensions of 9.45 $\times$ 18.5 mm. A microstrip-fed rectangular radiator, as well as a ground plane with a rectangle slit and an L- shaped stub, are included in the design. The author proposed and analyzed a bendy UWB antenna, protecting 3.06 to 13.58 GHz [5]. A UWB antenna working from 3.1 GHz to 11.3 GHz changed into evolved using Gharbi *et al.* on a felt fabric substrate [6]. The author presented a UWB antenna on FR4 and a denim substrate, running withinside the 3.1 to 11 GHz band for wearable IoTs [7]. Bekasiewicz and Koziel advanced a CPW-fed UWB antenna on a paper substrate, running in 3.2–30 GHz with substantial benefit for IoT applications [8]. A U-shaped antenna operates in the 3-8 GHz frequency range. Due to some drawbacks, the excitation through the coaxial feed line is not used [9]. In ''Compact Ultra-Wide Band MIMO Antenna System for Lower 5G Bands,'' using H. Al-Saif *et al.*, the authors endorse a planar antenna with ultrawideband traits for MIMO applications. Saha *et al.* supplied a bendy UWB antenna fabricated using a floor amendment and self-metallization method on a polyimide substrate, including a 1.35 to 16.40 GHz band [10]. Kumar *et al.*. evolved a graphene-assembled film primarily based on compact and low-profile ultra- extensive bandwidth (UWB) antenna protecting 4.1–8.0 GHz wearable applications [11].

In this communication, we have proposed an annular ring antenna with an array of metallic vias at the outer periphery. The proposed antenna has utilized a partial ground plane with an arc at the center. The work has optimized the outer radius of the annular ring to explore a specific resonating band as per applications. Lower order modes are excited by the loading of slots near the feed line and the changed ground plane, which helps achieve ultra-wideband. The lower order modes are excited by optimizing the radius of the metallic vias, and the closely spaced bands are merged to achieve ultra-wideband. The DGS and the inner radius of the annular ring increase antenna gain while suppressing Co and cross-pole isolation. The changed dimension defected ground, slot-loaded ARMSA achieves 108% percent fractional bandwidth ranging from 3.2-10.6GHz.

Contribution of work: Due to certain inherent restrictions for electrically tiny antennas, designing miniaturized UWB antennas is rather difficult. Reducing the structural size, for example, shortens the current channel and, as a result, degrades impedance matching at lower frequencies. We explain the structure of a tiny UWB monopole antenna for IoT applications, where careful design aimed at explicit footprint reduction while keeping acceptable electrical performance is critical in obtaining a small dimension.

Novelty of work: The disadvantage of employing an Omni-directional antenna, such as a dipole antenna connected to an IoT module, is that it has a low gain, resulting in limited system throughput. In addition, because the Omni-directional antenna may radiate in all directions, The co-channel may receive and transmit signals in all directions. Inference from other directions has become a significant issue. In addition, because the Internet of Things is a point-to-point link, An antenna can spatially be beaming all signals to

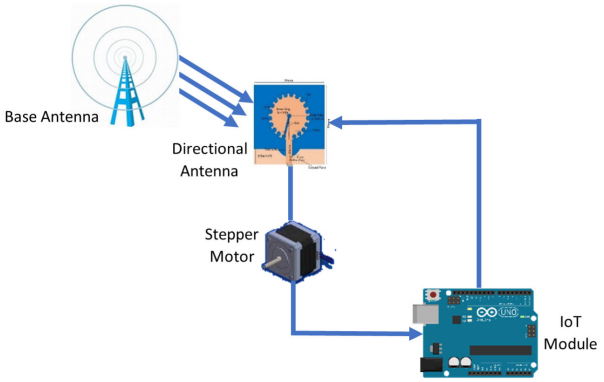

FIGURE 1. IoT system with directional antenna.

a single point. The destination is the main emphasis to prevent getting lost in useless space. As a result, a directional antenna is a good option. IoT is a network-based internet-of-things solution. One of the more intriguing directional antennas is the microstrip patch antenna, which has the benefit of being tiny size, low-profile, low-cost manufacture, and lightweight are all important factors. The mechanical system is designed and implemented for controlling the 360-degree rotation of the directional antenna using a stepping motor and microcontroller.

Algorithm to Control Stepper Motor with IoT and Arduino Uno Fig 1, the antenna receives a signal from the base station. It conveys the signal to the microcontroller, which contains Arduino and IoT modules. Then, the microcontroller stores the signal strength value and degree of rotation every 10 degrees, which means that we can store 36 values in one round. The microcontroller's algorithm compares the signal strength values. The main program makes an infinite loop that decides the maximum signal strength, as the flowchart is shown in Fig 2. These values are compared with previously stored values. When we give the maximum signal strength values, the stepper motor will rotate in the direction in which the antenna can receive maximum signal strength.

II. ANTENNA GEOMETRY AND PARAMETRIC ANALYSIS

A. ANTENNA GEOMETRY

Substrate selection: The foundation for producing high-performance integrated circuits and systems is low-loss material. As the frequency rises into the millimeter-wave regions and beyond, this becomes more important for the power budget. This is due to the difficulty of amplification over those ranges. For a better and more accurate design, consider the temperature effect, dielectric nonuniformity, and metallic surface roughness. This is very significant in the creation of antennas. The holes can be drilled mechanically with ease. In addition, the design should consider the material's thermal stability.

Geometry selection: The resonant frequency of Annular Ring Microstrip Antenna is lower than Rectangular Microstrip Antenna and Circular Microstrip antenna at the

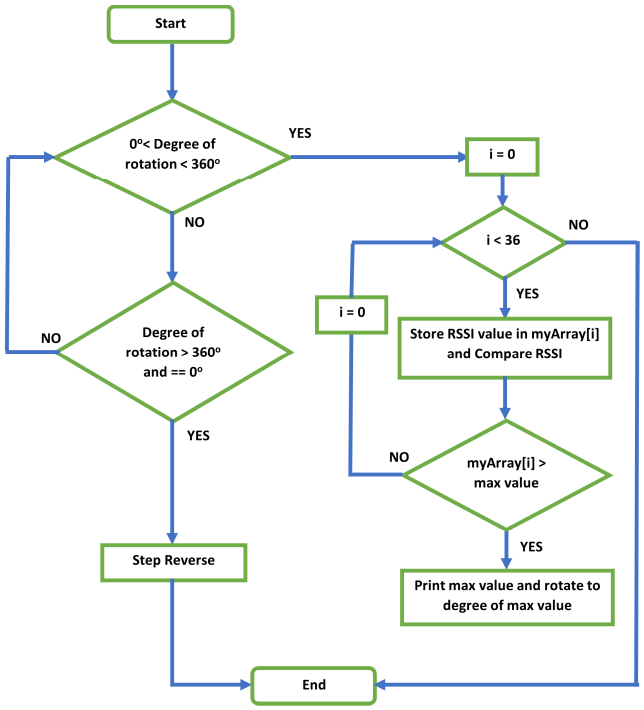

FIGURE 2. Flow chart of the algorithm used to determine the best recieved signal direction [24].

fundamental mode. Hence, ARMA can be used to design compact antennas preferred over RMA and CMA. In a fundamental mode, ARMA shows wider HPBW (104degree) in an e-plane, whereas the RMA shows wider HPBW (98degree) at an h-plane [12]. The ring's outer radius is denoted by a, and the width of the ring is w. The resonance frequency of the dominant mode of a circular disc is determined as follows

$$fr = \frac{(1.8421\ C)}{(2\pi a \epsilon_r)}, \tag{1}$$

Here, c is the velocity of light in the free space, a is the radius of the disc, and ϵ_r is the dielectric constant of the substrate. It can be shown that the resonance frequency of a circular ring is somehow less than that of the disc. If the ring gets narrower, its corresponding resonance frequency shifts, making more miniaturization. For example, if it is desired to have an annular ring antenna (ARA) to operate at 4.7 GHz, according to (1), the radius of the disc should be about 9.8 mm. It should be noted that in this calculation, the substrate FR4 (ϵ_r=4.4,h=1.6mm is selected.) The proposed antenna consists of an annular ring with outer radius (a) and inner radius (b), as in Fig.3. The metallic via array is included at the outer periphery of the annular ring at a separation of an angle 15degree. A rectangular slot with a width of 1mm, extending clockwise from the feed point towards the first via on the periphery, has been embedded in the configuration at an angle of 15 degrees from the middle of the patch. The ground of the proposed structure has been defected to provide good impedance matching and shift the return loss curve further towards the lower frequency band. The antenna

TABLE 1. Comparison of the proposed work with similiar performance work.

Publication	Gain	Cross polarization	Front to Back ratio	radiation pattern
[18]	7.94dBi at 3.64 GHz	high	low	Omnidirectional
[19]	3dBi	high	low	omnidirectional
[20]	5.8dBi	20dB	14dB	Omnidirectional
[21]	2.96dBi	high	low	Omnidirectional
[22]	5dBi	high	low	Omnidirectional
Proposed work	9dBi	low	34 dB (high)	Unidirectional

is fabricated on an FR4 substrate with a dielectric constant of 4.4 and a surface area size of 34 mm × 34 mm and 1.6 mm, respectively. The diameter of a metallic via (d) and patch outer radius fed employing a 50 ohm.

Diameter of hole $d < \lambda$ g/5, distance between center of two holes is $P <$ 2d. Shorting posts can also be used to vary the operating frequency of a patch antenna, and this frequency tuning is mainly a function of the number and location of the posts. The posts are placed along the edge of the patch and spaced equally apart. As the number of posts increases, the range over which the antenna's operating frequency can be varied becomes substantial. This frequency tuning is mainly a function of the number and location of the posts. These effects occur because the posts act like reactive elements, which modify the frequency variation with input impedance. The bandwidth without a metallic array is 76%, whereas when the patch is integrated with the metallic array, bandwidth enhances to 108%. This is not a substrate integrated waveguide structure as the need of this technique is that the vias are drilled between two metallic layers. Here, the ground layer is nonmetallic.

Varying the outer to inner radius ratio can manage the separation of resonant modes by changing the outer to inner radius ratio, an exciting feature of annular ring patches. Compared to a circular patch antenna, the proposed annular structure has a broader bandwidth and a smaller size shown in Figure 12 [4]. The current shield distribution in the ground plane is disturbed by an engraved periodic or non-periodic cascaded structure defected in the ground of a planar transmission line. A transmission line's properties are altered as a result of this disturbance. The value of line capacitance and inductance is changed due to the location of D.G.S., which causes the value of reactance to be set near zero to achieve impedance matching,shown in figure 12 where without defects in the ground, the S11 parameter just grazed −10dB. The presence of surface waves in the microstrip antenna is a significant problem that reduces the antenna's performance. The annular patch's slot is engraved to add extra resonance to the structure and increase bandwidth [13].

B. PARAMETRIC ANALYSIS

1) EFFECT OF ANNULAR RING PATCH

The radiating part is the annular ring patch. Figure 5 depicts the return loss curve and resonant frequency variance for various outer radius values ranging from 9.3mm to 10.3mm.

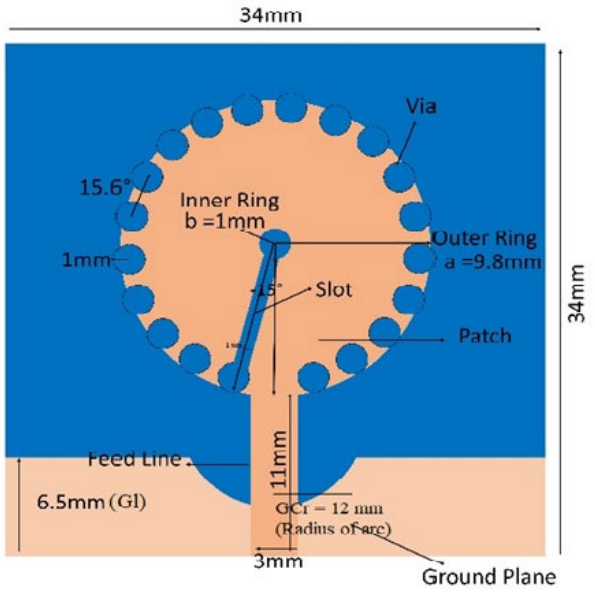

FIGURE 3. Geometry of the proposed antenna.

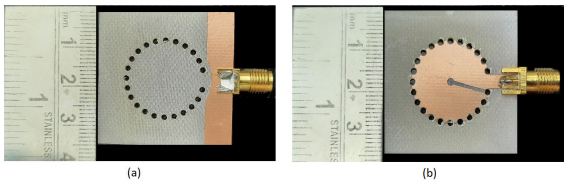

FIGURE 4. Fabricated prototype: a) Bottom side and b) Top side.

The antenna's impedance matching and bandwidth are affected by the radius of the outer circle [14]. As the outer radius (a) increases, the resonant frequency decreases, and the impedance matching deteriorates.

2) EFFECT OF DEFECTED GROUND STRUCTURE

The microstrip antenna's radiation characteristic is improved by using a defective ground structure to eliminate higher mode harmonics and cross-polarization. A slot cut technique often excites various modes, then combined using a faulty ground plane. As a result, the D.G.S. increases the bandwidth while simultaneously lowering the resonant frequency. The defected ground structure compensates for the inductive reactance with capacitive [15]. The length of the conductive area at the ground (Gl) and the radius of the arc cut at the

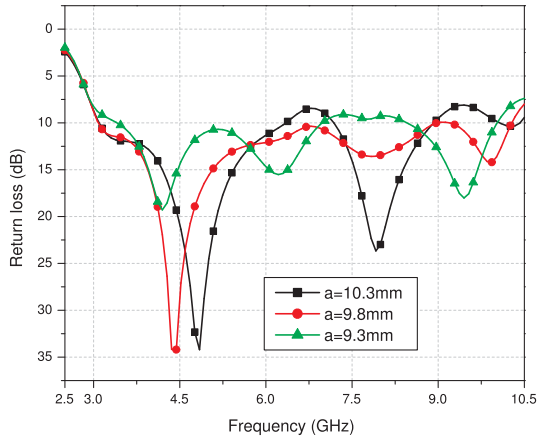

FIGURE 5. Variation of return loss with frequency for outer radius.

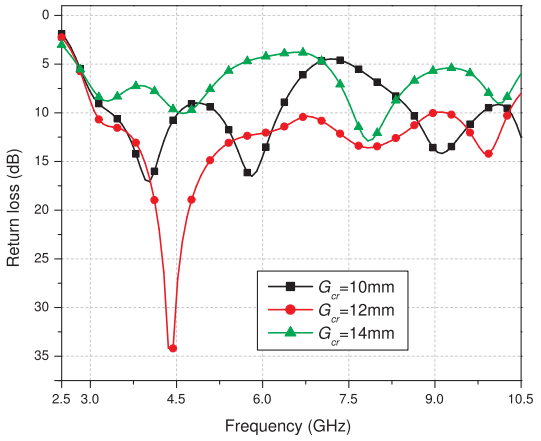

FIGURE 6. Variation of return loss with frequency for different radius of arc Gcr.

conductive strip at the bottom define a contaminated ground (GCr). For different values of the radius of the arc cut at the conductive strip at the ground, the return loss curve and resonant frequency shift (GCr). The Gcr values varied from 10 to 14 mm, and the corresponding return loss curves are shown in Fig.6.The structure becomes inductive as the value of Gcr increases, and the impedance matching suffers. The return loss and resonant frequency for different lengths (Gl) of the conductive region at the ground from 0.6 mm to 0.7 mm are shown in Fig 7. The reflection coefficient value is less than 40dB when Gl = 0.65 mm is used.

3) EFFECT OF RADIUS OF VIA

As the radii of the vias vary from 0.8 mm to 1.2 mm, the return loss varies, as shown in Figure 5. The modes are merged for via = 0.8 mm, resulting in return loss greater than 10 dB across the entire frequency range from 3.2 GHz to 10.6 GHz, contributing 108% fractional bandwidth. The simplest way to increase bandwidth is to increase antenna thickness while lowering substrate permittivity, which reduces the Quality factor. However, since the lowest substrate dielectric constant is 1, a thick substrate excites the surface wave, resulting in poor radiation efficiency and reduced permittivity; bandwidth increases due to the merging of the non-resonating waves. In the present work, an array of metallic via acts as a discontinuity in the path of the surface wave, which further merges to enhance the bandwidth of an antenna [16]. The fractional bandwidth of the antenna without using metallic via array is 76%, increasing up to 108% when the array is integrated.

4) EFFECT OF RECTANGULAR SLOT IN ANNULAR RING

A slot near the feed line has been etched to add extra resonance, enhancing the antenna's bandwidth in the desired frequency range [17]. Thus, tilting the rectangular slot provides impedance matching and maximizes gain. Figure 10 depicts the difference in return loss and resonant frequency for slot angles ranging from 10 to 20 degrees. The variance due to slot width is depicted in Figure 11.

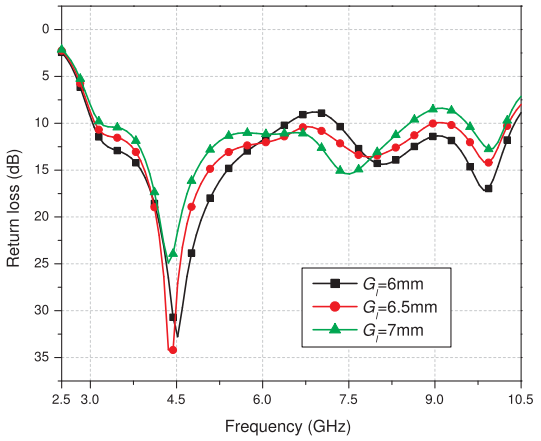

FIGURE 7. Variation of return loss with frequency for different conductive ground length.

Comparison of the return loss of the proposed structure without via array, DGS, and the slot with the proposed antenna is shown in Figure 12. Without a defective ground structure, the return loss's magnitude is much less. As metallic via array is added to the structure, it rigorously enhances the bandwidth and improves the gain. As the dielectric constant of the medium decreases by drilling the vias inside the substrate and results in an increase in bandwidth. The radiated power increases due to a decrease in stored energy, the quality factor decreases, and hence the bandwidth increases.

III. EQUIVALENT CIRCUIT

To investigate the behavior of the proposed antenna, the structure is analyzed with the help of an equivalent circuit model as in Fig. 13: An equivalent circuit model of the antenna is introduced for the calculation of input impedance matching, which is used to design an equivalent circuit of microstrip fed antenna. This model consists of a parallel RLC circuit in series with a reactance. This is usually modeled as a series inductor Lfeedline due to microstrip feed. Considering the desired output from the microstrip model, it can be deduced

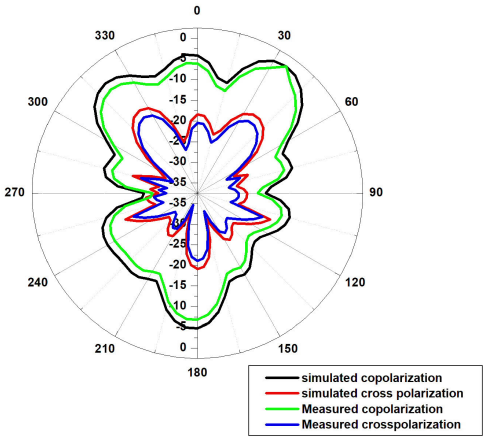

(a) At (3.87 GHz) XZ Plane

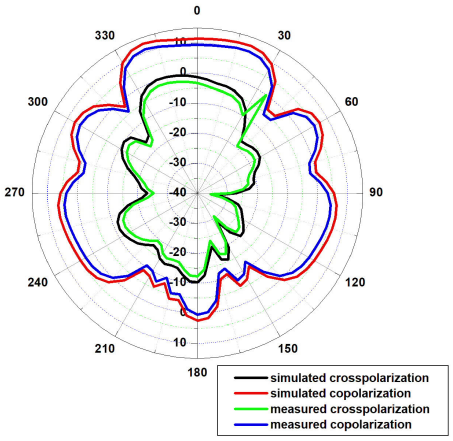

(b) At (5.24 GHz) XZ Plane

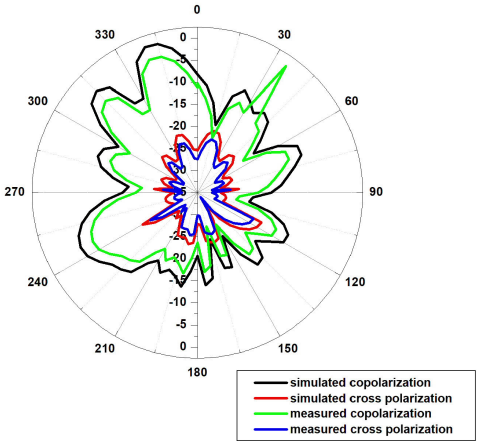

(c) At (7.21 GHz) XZ Plane

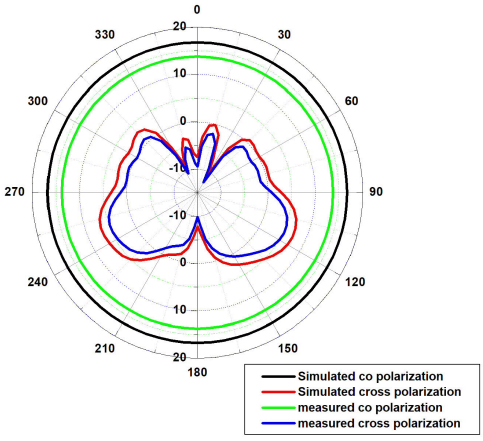

(d) At (5.24 GHz) YZ Plane

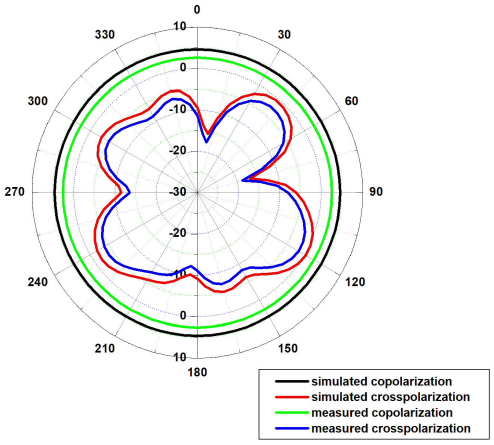

(e) At (3.87 GHz) YZ Plane

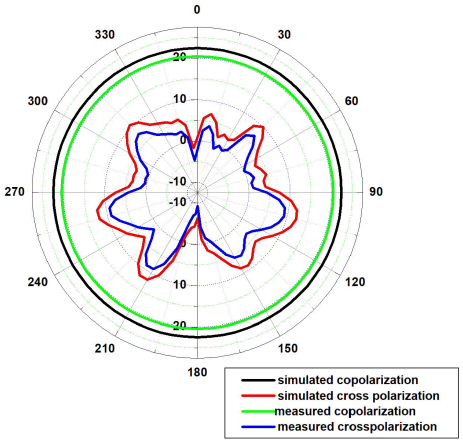

(f) At (7.21 GHz) XZ Plane

FIGURE 8. At (3.87 GHz) a) YZ plane, b) XZ plane. At 5.24 GHz c) YZ plane, d) XZ plane. At 7.21 GHz e) YZ plane, f) XZ plane.

that there is a direct relationship between the width of the feed (Wf) and the dielectric constant of the substrate ϵ_r, and the substrate height with the impedance of the antenna. If R1 is equal to 50 Ω in the RLC tank circuit.

The arrangement of elements in the equivalent circuit model is the same as the microstrip form in a nested structure. In this structure, the inner and outer circuits are related to the higher and lower frequencies, respectively, considering

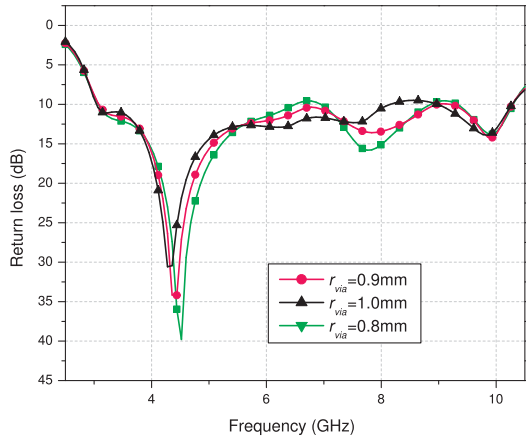

FIGURE 9. Variation of return loss with frequency for different radius of vias.

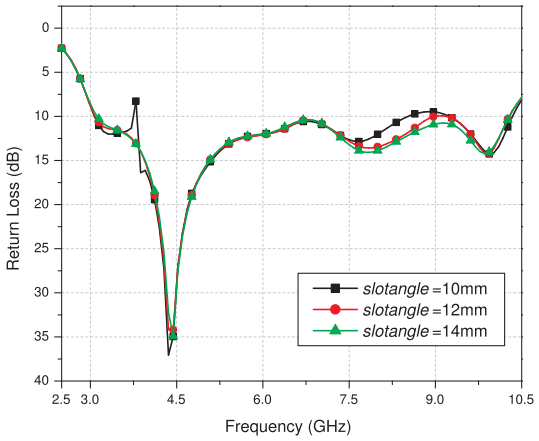

FIGURE 10. Variation of return loss with frequency for different slot angle.

figure 10. the highest and lowest resonant frequencies are achieved using RHCHLH and RLCLLL tank circuits, respectively. also R1C1L1, R2C2L2 .....Rn-1Cn-1Ln-1 generate n-1 frequency between fl & fH.The value of n depends on the type of design. The values of LCR can be obtained directly from the ADS software. A parallel RLC resonant circuit is used to model the antenna.

The annular patch with metallic via array equivalent R, L, and C are calculated using the S-matrix extracted from the HFSS. Agilent ADS is used to extract the equivalent circuit parameters. The input impedance of ARMSA can be written as follows.

$$Z_{in} = \frac{(R\omega^2L^2 + jR^2(\omega L - \omega^3L^2C))}{(R^2(1-\omega^2LC)^2 + \omega^2L^2)} \tag{2}$$

$\omega = 2\pi f$ f is the resonant frequency and R, L, C can be expressed as:

$$C = \frac{(\pi\epsilon_r\epsilon_o)}{(\epsilon n^2 h)} \tag{3}$$

$$L = \frac{(\epsilon n^2 h\mu_o)}{(\pi k^2)} \tag{4}$$

$$R = \frac{Q_o}{\pi fc} \tag{5}$$

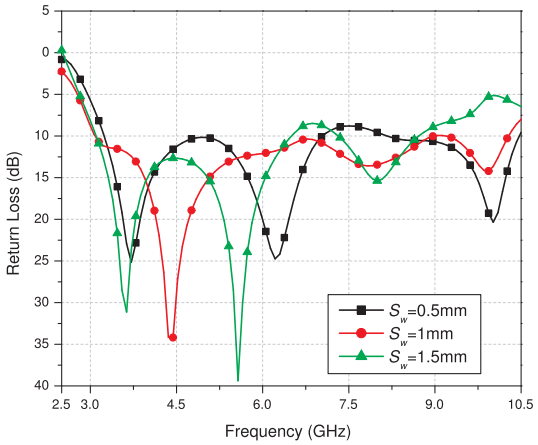

FIGURE 11. Variation of return loss with frequency for different slot width.

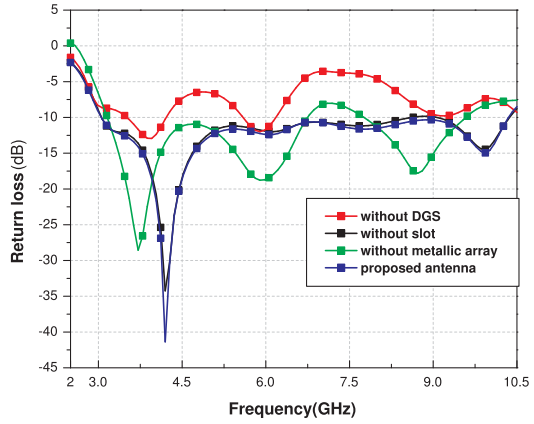

FIGURE 12. Comparison of the return loss of the proposed structure without via array, DGS, and the slot with the proposed antenna.

When a slot is inserted in microstrip feed ARMSA, The input impedance of the slotted microstrip feed ARMSA is represented as follows.

$$Z_{in} = \frac{1}{(R' + jwL' + (\frac{1}{jwC'}))} \tag{6}$$

R', L' and C' are the equivalent resistance, inductance & capacitance of a patch. The resonant frequency of annular ring antenna with metallic v is calculated as follows.

$$f_{r(mnp)} = \frac{(K_{mnp}C)}{(2\pi a\sqrt{(\mu_r\epsilon_r)})} \tag{7}$$

$$Q = \frac{F_r}{BW} = \omega_o\frac{L}{R} \tag{8}$$

where Q is the Quality factor, $Kmnp$ is the resonant wave number, a is the radius of the outer ring, BW is the bandwidth, Fr is the resonance frequency, ϵ_r is the relative permittivity, and Mur is the relative permeability. A small resistance Rl is included to represent the feed line. The proposed antenna is fed via a microstrip line, which acts as a current probe [7]. The annular ring patch is modeled as a voltage-driven current source, with a metallic through mounted on the top layer at the periphery. The resistance values of each

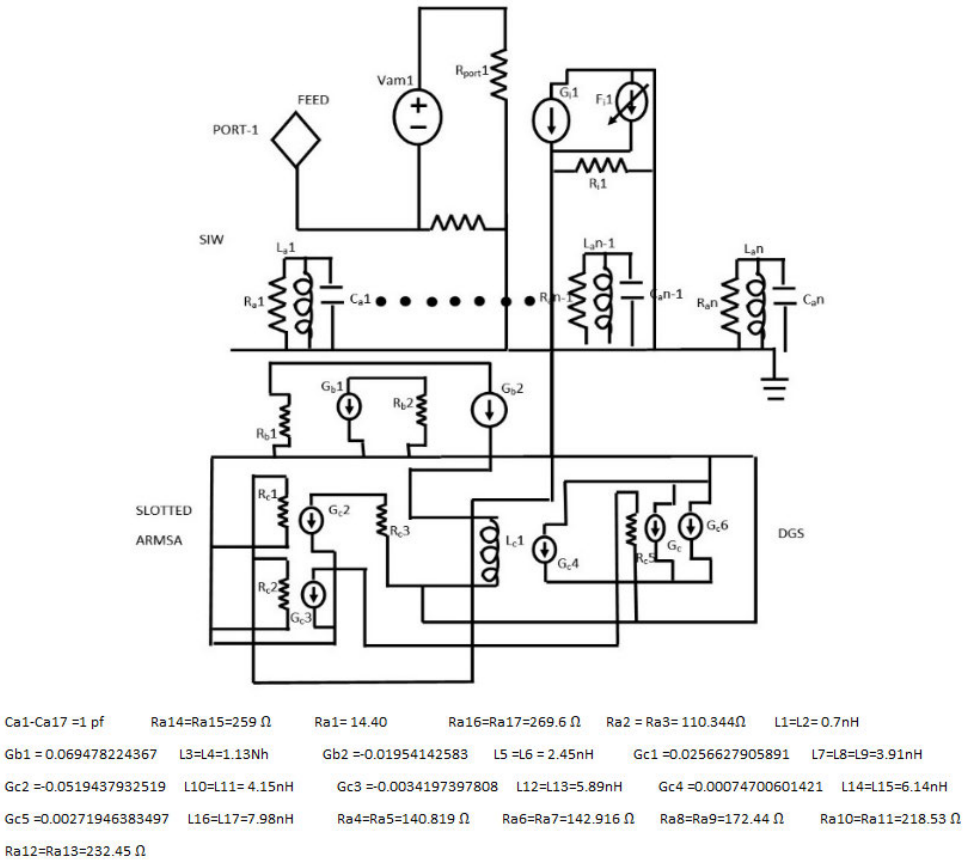

FIGURE 13. Equivalent circuit of proposed antenna.

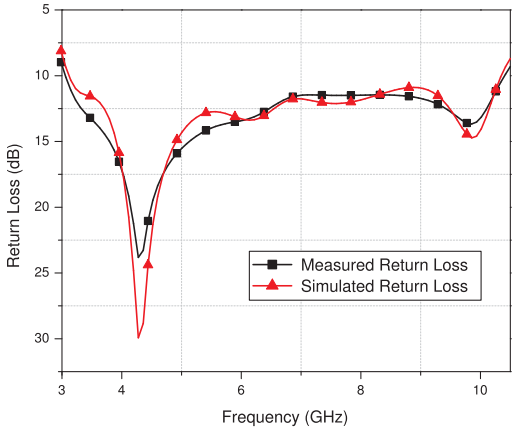

FIGURE 14. Variation of s11 with frequency simulated &measured result.

resonator are optimized using Agilent ADS software to achieve proper impedance matching. In addition, the proposed model includes a defective ground structure that alters the microstrip line's efficient capacitance and inductance.

IV. RESULT AND DISCUSSION

A. ELECTRICAL PROPERTIES OF THE STRUCTURE

Figures 14 and 17 show the simulated and measured return loss and gain of an ARMSA loaded with metallic via array using an Anritsu Vector Network Analyzer MS2037 C. On the top, the Surface current flows along the metal plane of the patch on the antenna. However, on the sides, surface current flows vertically along the metalized surface of the cylinders, which is minimally perturbed by the gaps. The electric field is normal to the broad wall, and its amplitude does not vary in the vertical direction. Moreover, the thickness h of the substrate plays no role in the characteristics of wave propagation, except the conductor losses. When an annular patch is loaded with metallic via array, TM22 & TM11 modes get excited.The field plot for all modes exists shown in figure 8, and there is no influence from other modes. the metallic via through an array is supposed to disturb and inhibit any orthogonal resonance from occurring. This reduces the cross-polarization level by weakening the fringing fields on the y-axis. This enhances the E/H wall or cross-polarization [23] Figures 16 and 17 depict the input impedance and gain of the proposed structure. Integration of metallic via array with annular ring microstrip antenna compensates the capacitive reactance with the equivalent inductive reactance to maintain the resonant frequency. With this modification, the real part of the impedance becomes 50 ohm, and the imaginary part becomes zero, and the bandwidth enhances to 108 %. The effect of the annular ring, ring slot, and shorting vias on the antenna's impedance

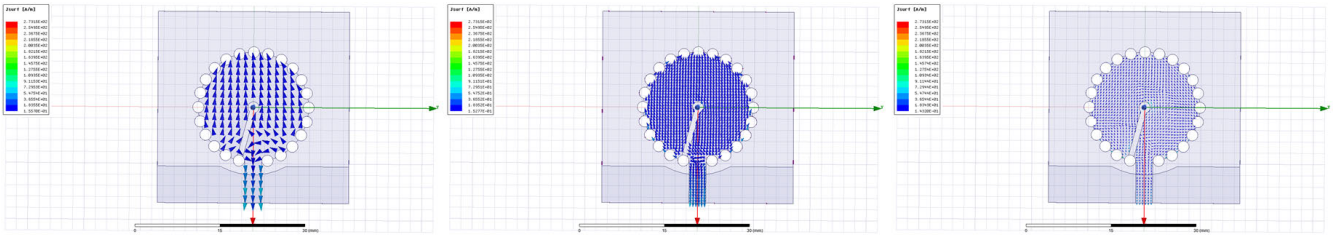

FIGURE 15. Surface current density at (a) 3.87 GHz (b) 5.24 GHz (c) 7.21 GHz.

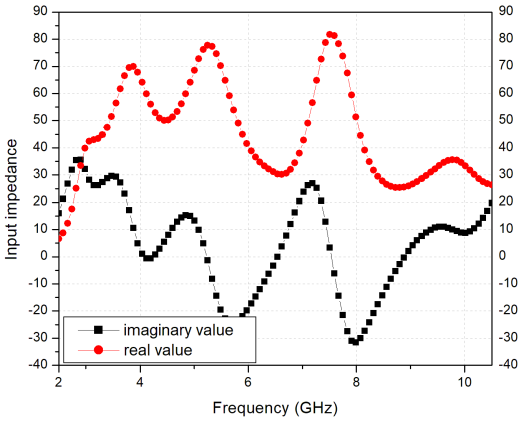

FIGURE 16. Variation of input impedance with frequency.

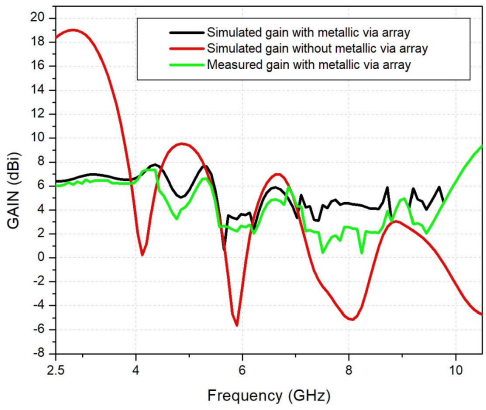

FIGURE 17. Variation of gain with frequency with and without metallic array.

bandwidth is depicted. The cavity model can be used to examine the resonant frequencies of the patch antenna since h (the thickness of the substrate) is very small compared to the wavelength in free space. The microstrip feed can trigger the TM11 mode for antennas with a smaller circular patch (without slot, annular ring, or shorting vias). The effective radius ae of the smaller circular patch can be calculated as follows, considering the fringing effect at the open edge.

$$ae = a\sqrt{1 + \frac{2h}{\pi a \epsilon_r}\left(ln\frac{\pi a}{2h} + 1.776\right)} \tag{9}$$

The resonant frequency for the TM11mode is

$$f_{cTM_{11}} = \frac{3.83171c}{2\pi a_e \sqrt{\epsilon_r}} \tag{10}$$

where c is the velocity of light. fc atTM11 is 5.4GHz. After the annular ring is introduced (with slot and without shorting vias), The TM11 mode of the annular ring is also excited. The resonant frequency for this TM11 mode can be calculated as follows.

$$f_{rTM_{11}} = \frac{c\chi}{2\pi r_1 \sqrt{\epsilon_r}} \tag{11}$$

where χ is the root of the characteristic equation.

B. RADIATION PATTERN, GAIN, FB RATIO

The section investigated the gain, front-to-back lobe radiation ratio (FBR), and the polarization characteristics of the

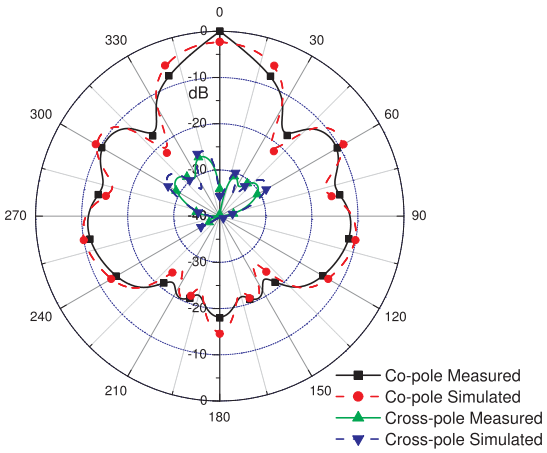

FIGURE 18. Antenna radiation pattern at 4.27 GHz in the xz plane.

antenna in the E plane and H plane at the desired band. An annular ring microstrip patch printed on the substrate with proposed D.G.S. and the Metallic vias of appropriate size strategically on the orthogonal plane does not affect the patch's dominant mode fields, nor do they influence the element's input impedance or cause any backward radiation.

The ground plane's edges and corners radiate the surface waves. The combined radiation from the patch and the ground plane edges form a series of neutralized lobes by eliminating a

TABLE 2. Comparison of proposed work with previous published work.

Publication	Permittivity	Size(mm)	Frequency range(GHz)	FBW	Peak Gain	Material
[3]	3.2	34 × 25	1.66–16.1	188.5	4.91	PET Paper
[4]	2.08	45 × 35	1.20–13.0	166.2	5.40	Teflon
[5]	2.65	32 × 24	2.70–12.0	-	3.80	-
[6]	3.00	23 × 20.2	3.00–20.0	-	4.40	Tape
[7]	3.40	47 × 33	2.20–14.3	-	4.95	Kapton polyimide
[1]	3.50	38 × 30.4	2.85–19.4	-	4.15	Kapton polyimide
[10]	4.40	24 × 31	3.05–12.9	-	4.70	FR4
[Proposed work]	4.40	34 x 34	3.1-10.3	108	9	FR4

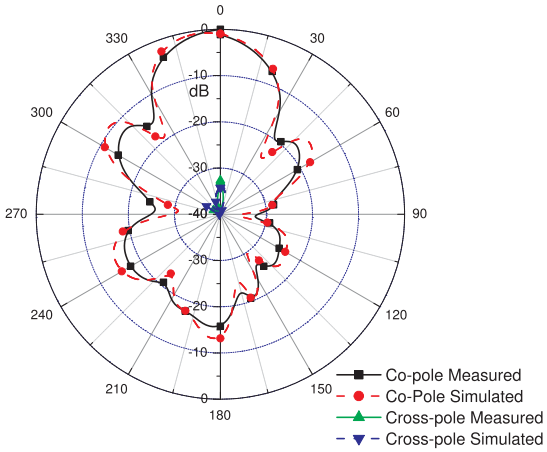

FIGURE 19. Antenna radiation pattern at 4.27 GHz in the yz plane.

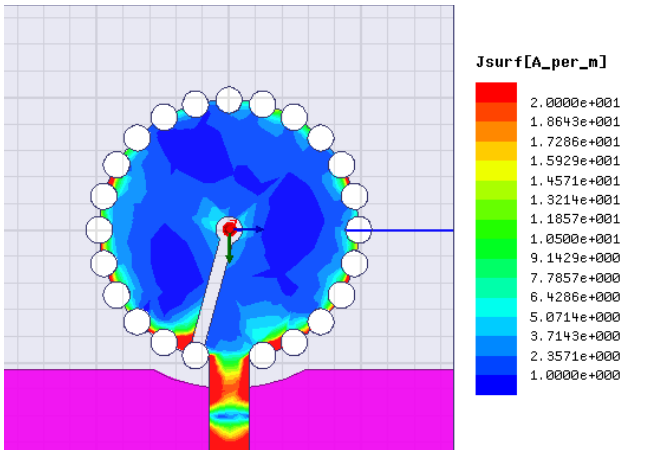

FIGURE 21. Surface current distribution of the proposed antenna.

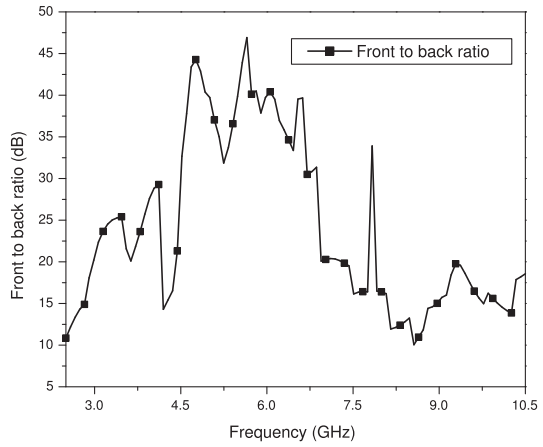

FIGURE 20. Front to back ratio.

portion of the ground plane. Some parts of the radiated power from the ground plane edges and corners are propagated through a metallic via improving the Front to back ratio. The simulated gain attains the peak value of around 10 dBi at the resonance frequency. The measured result of antenna gain is very close to the simulated results.To enhance the bandwidth, holes are drilled along the periphery of the annular ring. Due to this discontinuity, mode changes frequently result in gain instability.Optimization of parameters is done to enhance the gain. The far-field radiation pattern of the proposed antenna for both E- and H-planes at resonant frequency 4.27 GHz are shown in Figures 18 and 19, respectively. It is observed that simulated results of both E- and H-planes are in good agreement with the experimental results. The cross-polarization level in E- plane is suppressed by 30dB in the E plane and 40dB in the H plane, respectively. It should be noted that the H-plane cross-polarization level is relatively low. Figure 20 shows that the FBR of the proposed antenna is more than 20 dB for the entire band and 34dB at the resonant frequency. Figure 21 has studied the surface current distribution of the proposed antenna.

V. CONCLUSION

DGS integrated SIW ARMSA with micro stripline feeding is presented in the paper. It is observed that the radiation properties of the slot-loaded SIW ARMSA are highly affected by the defected ground structures, inner and outer radius of the annular ring and the radius of the metallic vias. The study has revealed that the outer radius affects the highest resonating frequency while the inner radius influences the gain. The slot, partial ground plane with central arc enhances the gain, excites lower order modes, and suppresses the Co and X polarized isolation. Finally, the metallic vias stimulate newer modes and merge all the closely spaced modes to proffer ultra wideband. The design has an impedance bandwidth of about 108% with a central frequency of 4.27 GHz. For the entire band, the gain obtained is found 10dBi. The structure

offers Front to back ratio of 34 dBi and 97% efficiency at the resonant frequency. Ultra-wideband applications may utilize the proposed antenna for Ultra Wide Band Applications.

REFERENCES

[1] C.-C. Chong, F. Watanabe, and H. Inamura, "Potential of UWB technology for the next generation wireless communications," in *Proc. IEEE 9th Int. Symp. Spread Spectr. Techn. Appl.*, Manaus, Brazil, Aug. 2006.

[2] S. Duenas, "Design of a DS-UWB transceiver," KTH Roy. Inst. Technol., Stockholm, Sweden, 2006.

[3] C. Jin, Z. X. Shen, R. Li, and A. Alphones, "Compact circularly polarized antenna based on quarter-mode substrate integrated waveguide sub-array," *IEEE Trans. Antennas Propag.*, vol. 62, no. 2, pp. 963–967, Feb. 2014.

[4] S. Mukherjee and A. Biswas, "Computer aided equivalent circuit model of SIW cavity backed triple band slot antenna," *Int. J. RF Microw. Comput.-Aided Eng.*, vol. 27, no. 2, 2017, Art. no. e21060.

[5] Y. Zhang, S. Li, Z. Yang, X. Qu, and W. Zong, "A coplanar waveguide-fed flexible antenna for ultra-wideband applications," *Int. J. RF Microw. Comput.-Aided Eng.*, vol. 30, no. 8, 2020, Art. no. e22258, doi: 10.1002/mmce.22258.

[6] G. M. El, M. Martinez-Estrada, R. Fernández-García, S. Ahyoud, and I. Gil, "A novel ultra-wide band wearable antenna under different bending conditions for electronic-textile applications," *J. Textile Inst.*, vol. 112, no. 3, pp. 437–443, 2020, doi: 10.1080/00405000.2020.1762326.

[7] M. A. Peyrot-Solis, G. M. Galvan-Tejada, and H. Jardon-Aguilar, "State of the art in ultra-wideband antennas," in *Proc. 2nd Int. Conf. Electr. Electron. Eng.*, 2005, pp. 101–105.

[8] A. Bekasiewicz and S. Koziel, "Compact UWB monopole antenna for Internet of Things applications," *Electron. Lett.*, vol. 52, no. 7, pp. 492–494, 2016.

[9] M. Mustaqim, B. A. Khawaja, H. T. Chattha, K. Shafique, M. J. Zafar, and M. Jamil, "Ultra-wideband antenna for wearable Internet of Things devices and wireless body area network applications," *Int. J. Numer. Model., Electron. Netw., Devices Fields*, vol. 32, no. 6, p. e2590, 2019.

[10] T. K. Saha, T. N. Knaus, A. Khosla, and P. K. Sekhar, "A CPW-fed flexible UWB antenna for IoT applications," *Microsyst. Technol.*, vol. 28, no. 1, pp. 5–11, Jan. 2022.

[11] A. Kumar, J. Kaur, and R. Singh, "Performance analysis of different feeding techniques," *Int. J. Emerg. Technol. Adv. Eng.*, vol. 3, no. 3, pp. 884–890, Mar. 2013.

[12] S. B. Glybovski, V. P. Akimov, and A. E. Popugaev, "Analytical study of annular-ring microstrip antennas shorted with thin wires," *IEEE Trans. Antennas Propag.*, vol. 62, no. 6, pp. 3348–3353, Jun. 2014.

[13] F. Wang and T. Arslan, "A wearable ultra-wideband monopole antenna with flexible artificial magnetic conductor," in *Proc. Loughborough Antennas Propag. Conf. (LAPC)*, Leicestershire, U.K., Nov. 2016, pp. 1–5.

[14] H. Dashti and M. H. Neshati, "Development of low-profile patch and semi-circular SIW cavity hybrid antennas," *IEEE Trans. Antennas Propag.*, vol. 62, no. 9, pp. 4481–4488, Sep. 201.

[15] V. Kumar and B. Gupta, "On-body measurements of SS-UWB patch antenna for WBAN applications," *AEU - Int. J. Electron. Commun.*, vol. 70, no. 5, pp. 668–675, May 2016, doi: 10.1016/j.aeue.2016.02.003.

[16] H. R. Khaleel, H. M. Al-Rizzo, D. G. Rucker, and S. Mohan, "A compact polyimide-based UWB antenna for flexible electronics," *IEEE Antennas Wireless Propag. Lett.*, vol. 11, pp. 564–567, 2012, doi: 10.1109/LAWP.2012.2199956.

[17] W.-C. Liu and P.-C. Kao, "CPW-fed triangular monopole antenna for ultra-wideband operation," *Microw. Opt. Technol. Lett.*, vol. 47, no. 6, pp. 580–582, Dec. 2005, doi: 10.1002/mop.21235.

[18] M. M. Sharma, A. Kumar, S. Yadav, and Y. Ranga, "An ultra-wideband printed monopole antenna with dual band-notched characteristics using DGS and SRR," *Proc. Technol.*, vol. 6, pp. 778–783, Jan. 2012, doi: 10.1016/j.protcy.2012.10.094.

[19] M. Rahman, M. NagshvarianJahromi, S. Mirjavadi, and A. Hamouda, "Compact UWB band-notched antenna with integrated Bluetooth for personal wireless communication and UWB applications," *Electronics*, vol. 8, no. 2, p. 158, Feb. 2019, doi: 10.3390/electronics8020158.

[20] K. Y. Kapusuz, S. Lemey, A. Petrocchi, P. Demeester, D. Schreurs, and H. Rogier, "Polarization reconfigurable air-filled substrate integrated waveguide cavity-backed slot antenna," *IEEE Access*, vol. 7, pp. 102628–102643, 2019, doi: 10.1109/ACCESS.2019.2926809.

[21] A. A. Adam, S. K. A. Rahim, K. G. Tan, and A. W. Reza, "Design of 3.1–12 GHz printed elliptical disc monopole antenna with half circular modified ground plane for UWB application," *Wireless Pers. Commun.*, vol. 69, pp. 535–549, 2013, doi: 10.1007/s11277-012-0588-4.

[22] T. Nahar and S. Rawat, "Survey of various bandwidth enhancement techniques used for 5G antennas," *Int. J. Microw. Wireless Technol.*, vol. 14, no. 2, pp. 204–224, Mar. 2022, doi: 10.1017/S1759078720001804.

[23] M. R. Hasan, M. A. Riheen, P. Sekhar, and T. Karacolak, "Compact CPW-fed circular patch flexible antenna for super-wideband applications," *IET Microw., Antennas Propag.*, vol. 14, no. 10, pp. 1069–1073, 2020, doi: 10.1049/iet-map.2020.0155.

[24] T. Kamolklang, A. Junlasat, and M. Uthansakul, "NB-IoT system performance enhancement using directional antenna," in *Proc. 11th Int. Conf. Inf. Technol. Electr. Eng. (ICITEE)*, Oct. 2019, pp. 1–6, doi: 10.1109/ICITEED.2019.8929983.

INDERPREET KAUR received the B.Tech. and M.Tech. degrees from Uttar Pradesh Technical University, Lucknow, India, in 2004 and 2011, respectively. She is currently a Research Scholar with the Department of Electronics and Communication Engineering, NIT Silchar, Assam, India. She is working as an Assistant Professor (stage3) with the Department of Electronics and Communication Engineering, Mahatma Jyotiba Phule Rohilkhand University, Bareilly. Her research interests include RF engineering, antenna designing, and the Internet of Things (IoT).

BANANI BASU (Senior Member, IEEE) received the bachelor's degree in technology from the Jalpaiguri Government Engineering College, in 2004, the master's degree in technology from the WB University of Technology, in 2008, and the Ph.D. degree from the National Institute of Technology Durgapur, in 2012. She is currently working as an Assistant Professor (Grade I) with the National Institute of Technology Silchar, Assam, India. Her research interests include antenna design, machine learning, and metamaterial-inspired structures.

ANIL KUMAR SINGH received the Ph.D. degree from IIT (ISM) Dhanbad, India, in 2016. He is currently working as an Associate Professor with the Department of Electronics and Instrumentation Engineering, Faculty of Engineering and Technology, Mahatma Jyotiba Phule (MJP) Rohilkhand University, Bareilly. He has more than 18 years Teaching and Research Experience. He has more than 50 research publication in various reputed journals. He is a reviewer of many international journals. His research interest includes antenna engineering.

VINAY RISHIWAL (Senior Member, IEEE) received the bachelor's degree in engineering in computer science and engineering from the SRMS College of Engineering and Technology, Mahatma Jyotiba Phule (MJP) Rohilkhand University, Bareilly, India, in 2000, and the Ph.D. degree from Gautam Buddh Technical University, Lucknow, India, in 2011. He is currently working as a Professor with the Department of Computer Science and Information Technology, Faculty of Engineering and Technology, Mahatma Jyotiba Phule (MJP) Rohilkhand University. He has 21 years Teaching and Research Experience. He has published more than 90 research papers in various journals and conferences of international repute. His current research interests include wireless sensor networks, the Internet of Things (IoT), cloud computing, social networks, and blockchain technology. He is a Senior Member of ACM and also served as a Convenor, Student Activities Committee, and IEEE Uttar Pradesh Section. He has received many awards as best paper and best orator in various conferences. He is the General/Conference Chair of four International Conferences namely ICACCA, IoT-SIU, MARC 2020, and ICAREMIT. He has visited many countries for academic purposes and worked upon many projects of MHRD and UGC. He has been invited as keynote Speaker in many National/International Conferences/Seminars/Workshops/FDPs and STCs held in India and abroad.

SUDEEP TANWAR (Senior Member, IEEE) is currently working as a Professor with the Department of Computer Science and Engineering, Institute of Technology, Nirma University, India. He is also a Visiting Professor at Jan Wyzykowski University, Polkowice, Poland; and the University of Pitesti, Pitesti, Romania. He has authored two books, edited 13 books, and more than 270 technical papers, including top journals and top conferences, such as IEEE TRANSACTIONS ON NETWORK SCIENCE AND ENGINEERING, IEEE TRANSACTIONS ON VEHICULAR TECHNOLOGY, IEEE TRANSACTIONS ON INDUSTRIAL INFORMATICS, IEEE WIRELESS COMMUNICATIONS, IEEE NETWORK, ICC, GLOBECOM, and INFOCOM. He initiated the research field of blockchain technology adoption in various verticals, in 2017. His H-index is 54. He actively serves his research communities in various roles. His research interests include blockchain technology, wireless sensor networks, fog computing, smart grid, and the Internet of Things (IoT). He is a member of the Technical Committee on Tactile Internet of the IEEE Communication Society. He is a Senior Member of CSI, IAENG, ISTE, and CSTA. He has been awarded the Best Research Paper Awards from IEEE GLOBECOM 2018, IEEE ICC 2019, and Springer ICRIC-2019. He has served many international conferences as a member of the Organizing Committee, such as the Publication Chair for FTNCT-2020, ICCIC 2020, and WiMob2019; a member of the Advisory Board for ICACCT-2021 and ICACI 2020; the Workshop Co-Chair for CIS 2021; and the General Chair for IC4S 2019 and 2020 and ICCSDF 2020. He is also serving on the editorial boards for *Frontiers of Blockchain*, *Cyber Security and Applications*, *Computer Communications*, the *International Journal of Communication Systems*, and *Security and Privacy*.

GULSHAN SHARMA received the B.Tech., M.Tech., and Ph.D. degrees. He is currently working as a Senior Lecturer with the Department of Electrical Engineering Technology, University of Johannesburg. His research interests include power system operation and control and application of AI techniques to power systems. He is a Y Rated Researcher from NRF South Africa. He is working as an Academic Editor of *International Transactions on Electrical Energy System* (Wiley) and a Regional Editor of *Recent Advances in Electrical and Electronics Engineering* (Bentham Science).

PITSHOU N. BOKORO received the M.Phil. degree in electrical engineering from the University of Johannesburg, Johannesburg, South Africa, in 2011, and the Ph.D. degree in electrical engineering from the University of the Witwatersrand, in 2016. He is currently an Associate Professor with the University of Johannesburg. His research interests include modelling and reliability prediction of insulating materials and dielectrics, power quality, and renewable energies. He is a Senior Member of the South African Institute of Electrical Engineers.

RAVI SHARMA is currently working as a Professor with the Centre for Inter-Disciplinary Research and Innovation, University of Petroleum and Energy Studies, Dehradun, India. He is passionate in the field of business analytics and worked in various MNCs, as a Leader of various software development groups. He has contributed various articles in the area of business analytics, prototype building for startup, and artificial intelligence. He is leading academic institutions as a Consultant to uplift research activities in inter-disciplinary domains.